

Synthesis, characteristic, and flammability of modified carbon nanotube/poly(ethylene-*co*-vinyl acetate) nanocomposites containing phosphorus and silicon

Lichun Wang · Jinhong Yu · Zongliu Tang ·
Pingkai Jiang

Received: 22 April 2010/Accepted: 8 July 2010/Published online: 6 August 2010
© Springer Science+Business Media, LLC 2010

Abstract A novel flame retardant containing phosphorus–silicon, spirocyclic pentaerythritol bisphosphorate disphosphorylchloride/9,10-dihydro-9-oxa-10-phosphaphanthrene-10-oxide/vinyl methyl dimethoxysilane (SPDV), has been used to modify multiwalled carbon nanotubes (MWNTs) and the m-MWNTs (MWNTs-*g*-SPDV) was obtained by the covalent grafting of SPDV onto the surfaces of MWNTs. And then the according poly(ethylene-*co*-vinyl acetate) nanocomposites were prepared via melt blending. Transmission electron microscopy (TEM) results showed that a core–shell nanostructure with MWNTs as the hard core and SPDV as the soft shell was formed, and the resultant m-MWNTs can achieve better dispersion than pristine MWNTs in EVM matrix. Cone calorimeter results showed that better flame retardancy was obtained for EVM/m-MWNTs nanocomposites. Mechanical measurements showed that the Young’s modulus increases due to the presence of MWNTs or m-MWNTs. The flammability and mechanical properties of the nanocomposites are strongly dependent on the dispersion state of nanotubes.

Introduction

In recent years, the researches about carbon nanotubes (CNTs) have been a major interest since 1991 [1]. It is well-known that CNTs have unusual structural, electronic, mechanical, and

thermal properties, which provide great potential in a wide range of applications ranging from nanodevices to nanocomposites over the past number of years [2–6]. One of the major challenges is actually to easily and individually disperse these CNTs in polymer matrices to obtain materials with improved properties for different applications. Thus, many research groups have focused on the functionalization of CNTs with various organic, inorganic, and organometallic structures using both non-covalent and covalent approaches to improve the compatibility with polymer matrix [7–10]. Functionalization of CNTs with polymers is gaining particular interest because the long chains of polymer will help CNTs dissolve and disperse in good solvents and polymer matrix. Various methods, such as reversible addition–fragmentation chain transfer (RAFT) polymerization [11–13], atom transfer radical polymerization (ATRP) [14–18], irradiation polymerization [19], in situ surface electrografting [20], etc., have been developed for functionalizing CNTs. Recently, it appears interesting to use CNTs at low-loading content to obtain materials with enhanced mechanical properties or reduced flammability [21–26].

Various environmental friendly halogen-free flame retardants containing phosphorus and silicon elements have been developed due to their excellent carbonization and flame retardancy. In a previous research [27], a novel phosphorus–silicon containing flame retardant, spirocyclic pentaerythritol bisphosphorate disphosphoryl chloride/9,10-dihydro-9-oxa-10-phosphaphanthrene-10-oxide/vinyl methyl dimethoxysilane (SPDV), has been successfully synthesized and used in ethylene–vinyl acetate copolymer rubber (EVM). This study aims to modify multiwalled carbon nanotubes (MWNTs) with SPDV and prepare according EVM/MWNTs nanocomposites. It is anticipated that the covalent graft of SPDV onto MWNTs can improve the compatibility and dispersion of MWNTs in EVM

L. Wang · J. Yu · Z. Tang · P. Jiang
School of Chemistry and Chemical Engineering, Shanghai Jiao Tong University, Shanghai 200240, People’s Republic of China

L. Wang · J. Yu · Z. Tang · P. Jiang (✉)
Shanghai Key Lab of Electric Insulation and Thermal Aging,
Shanghai 200240, People’s Republic of China
e-mail: pkjiang@sjtu.edu.cn

matrix, and accordingly promote the flame retardancy of EVM/MWNTs nanocomposites.

Experimental

Materials

Poly(ethylene-*co*-vinyl acetate) (EVM) rubber (Levaprene 500HV) was kindly supplied by Bayer Co., Germany. The vinyl acetate content was 50 wt%, the Mooney viscosity was ML_{1+4} (100 °C) = 27 ± 4, the MFI (g/10 min) ≤ 5, and the density was 1.00 g/cm³.

Two types of MWNT (pristine MWNT and functionalized MWNT with hydroxyl group: MWNT-OH) with the same aspect ratios (outer diameter 10–20 nm, inner diameter 5–10 nm, length 10–30 μm) synthesized by chemical vapor deposition were purchased from Chengdu Organic Chemistry Co. Ltd., Chinese Academy of Science.

Dicumyl peroxide (DCP) was obtained from Shanghai Gaoqiao Petroleum Co. Ltd, China.

9,10-Dihydro-9-oxa-10-phosphaphenanthrene-10-oxide (DOPO) was purchased from Shandong Mingshan Chemical Co. Ltd., China.

Vinylmethyldimethoxy silane (VMDMS; Brand: SIL-QUEST A2171) was acquired from GE silicones.

Potassium hydroxide (KOH), acetonitrile (CH₃CN), chloroform (CHCl₃), triethylamine, toluene, acetone, and pentaerythritol (PER) were acquired from Shanghai Chemical Co. Ltd., China.

Aminopropyl triethoxysilane (APTES) were purchased from Acros and without purification.

Phosphorus oxychloride (POCl₃) was purchased from Tingxin Chemical Industry Co. Ltd., China.

Synthesis of spirocyclic pentaerythritol bisphosphorate disphosphoryl chloride/9,10-dihydro-9-oxa-10-phosphaphanthrene-10-oxide/SPDV [27]

A total of 100 mL acetonitrile, 14.8 g SPDPC (0.05 mol), and 31.1 g DV (0.05 mol) were introduced into a 250 mL three-neck and round-bottom glass flask with a mechanical stirrer, a thermometer, condenser, and a heating bath. The mixture was stirred for about 2 h at room temperature. Afterward, the mixture was gradually heated to 90 °C and refluxed until no HCl gas was emitted. The reaction would be completed after 12 h at 90 °C, when no HCl gas could be detected by the PH value measuring. It was then cooled to room temperature. Finally, the solvent was removed by the vacuum-pumping. The purified product was a flaxen solid. The synthesis route for SPDV was shown in Fig. 1a.

Synthesis of the MWNT-*g*-SPDV samples

5.0 g MWNT-OH were added to 250 mL of anhydrous toluene under N₂ atmosphere in a 500 mL flask with a reflux condenser. APTES was injected into the reaction system and refluxed at 80 °C for 24 h. The resultant was ultrasonically washed with toluene and acetone to remove any unreacted silane coupling agents. The APTES modified MWNT-OH

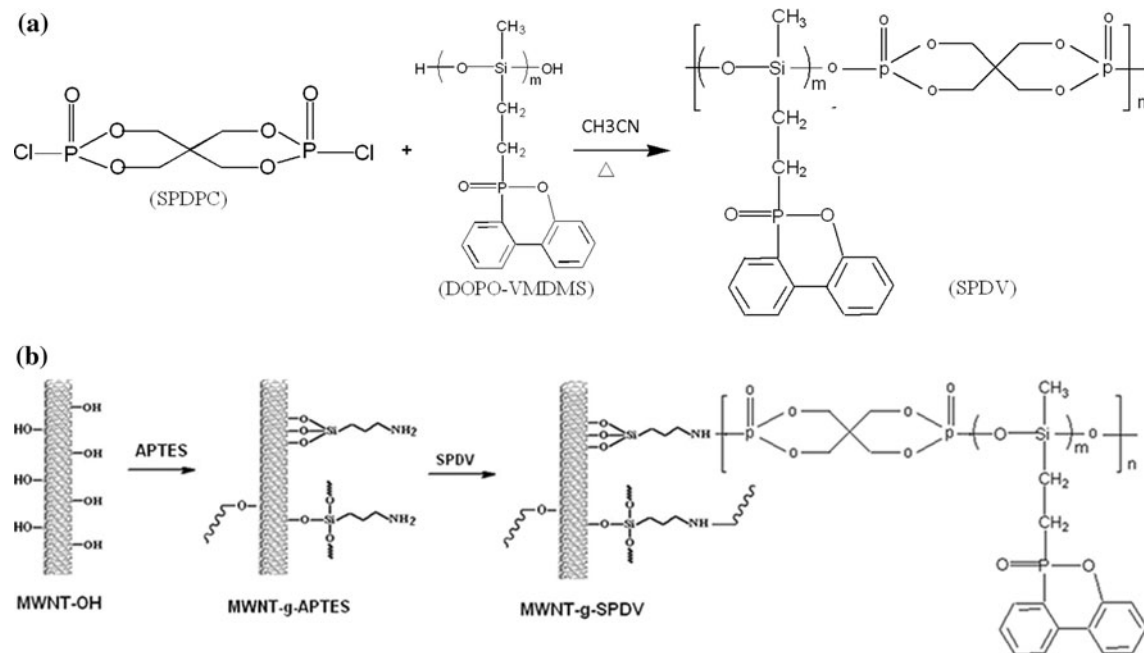


Fig. 1 The synthesis route of SPDV (a) and MWNT-*g*-SPDV (b)

(MWNT–NH₂) were obtained and dried under vacuum. Then the mixture of MWNT–NH₂, anhydrous acetonitrile, and triethylamine were added into a 150 mL flask and dispersed in ultrasonic bath for 2 h. Then acetonitrile solution of SPDV was added dropwise at 0 °C within 1 h. The mixture was stirred for 2 h at 0 °C, followed by stirring at room temperature for 48 h. The resultant MWNT-g-SPDV were obtained and washed with acetonitrile and dried under vacuum. The synthesis route for MWNT-g-SPDV was shown in Fig. 1b. The FTIR, ¹H NMR spectra, and transmission electron microscopy (TEM) were used to characterize the organically modified MWNT. The grafted SPDV content of MWNT-g-SPDV (m-MWNT) was determined by thermogravimetric analysis (TGA).

Preparation of EVM/MWNT nanocomposites

EVM pallets were dried at 40 °C in a vacuum for 6 h before processing to remove moisture. Then the EVM-based nanocomposites (filled with 2.0 phr DCP and 1.0 phr MWNTs or 1.0 phr m-MWNTs) were prepared in a Brabender internal mixer at 105 °C for 10 min with a speed of 50 rpm. The mixed samples were transferred to a mold and pressed at 175 °C for 10 min, and successively cooled to room temperature while maintaining the pressure (12 MPa) to obtain the nanocomposite sheets for further measurements.

Measurement and characterization

FTIR and ¹H NMR spectroscopy

The structure of SPDV and MWNT-g-SPDV was characterized by hydrogen nuclear magnetic resonance (¹H NMR), which were performed on an Mercuryplus 400 (300 MHz) NMR spectrometer with DMSO-*d*₆ as a solvent. The FTIR spectra of MWNT, MWNT-g-APS, and MWNT-g-SPDV were recorded with KBr powder by using a Perkin-Elmer Paragon 1000 instrument.

TEM

Morphological observation for MWNT, MWNT-g-SPDV and their dispersion in the EVM matrix were performed with a JEM 2100 transmission electron microscope. The EVM/MWNT nanocomposites samples were cooled at –80 °C and then microtomed with a diamond knife to give sections with a nominal thickness of 50–150 nm and 1 mm² of superficial area.

TGA

The TGA data were obtained in N₂ at a heating rate of 20 °C/min by a Perkin-Elmer Q 50 thermogravimetric

analyzer. In each case, a 5–10 mg sample was examined under the N₂ flow rate of 5 × 10^{–5} m³/min at the temperatures ranging from room temperature to 800 °C.

Cone calorimeter test

Cone calorimeter uses a truncated conical heater element to irradiate test specimens at heat fluxes from 10 to 100 kW/m², thereby simulating a range of fire intensities. The technique is a small-scale fire test, but it has been shown to provide data that correlate well with those from full-scale fire tests [28]. Cone calorimeter tests were carried out in duplicate, using a 35 kW/m² incident heat flux, following the procedures indicated in the ISO 5660 standard with a FTT cone calorimeter [29]. Each specimen, of dimensions 100 × 100 × 3 mm³, was wrapped in aluminum foil and placed on a mineral fiber blanket with the surface level with the holder, such that only the upper face was exposed to the radiant heater. The experimental error rate from the cone calorimeter test was about ±5%. The cone calorimeter technique provides detailed information about ignition behavior, heat release and smoke evolution during sustained combustion and some key parameters which are correlated well with real fire [30, 31].

Microstructure analyses by SEM

Scanning electron microscopy (SEM) analyses for the morphology of residues of combustion by cone calorimeter were made using a field emission scanning electron microscopy (FE-SEM, JEOL JEM-4701). The gold-coated samples to avoid accumulation of charges were analyzed at an accelerating voltage of 5.0 kV.

Mechanical measurements

The tensile properties of EVM/MWNT nanocomposites samples were measured on an Instron series IX 4465 material tester at a crosshead speed of 500 mm/min with dumbbell specimens (4 mm wide in the cross-section) according to ASTM D 412-06a. All the tests were carried out at 25 ± 2 °C.

Results and discussion

Synthesis and characterization of MWNT-g-SPDV

There are some of C–OH groups existing on the surface of obtained MWNT–OH and they provide the potentiality to further modify the MWNTs with organosilanes. Thus, the inorganic hydroxyl groups on surface of MWNT–OH are transformed into the more reactive organic amino

functional groups for further functionalization. The scheme to modify MWNTs is described in Fig. 1a and b. Figure 1a shows the synthesis route of SPDV which was obtained by the polycondensation of SPDPC and DV. The product was characterized by FTIR and NMR spectroscopy [27]. FTIR (KBr cm^{-1}): 3427 (Si–OH, end group in SPDV), 3074 (C–H in phenyl group), 2800–3000 (CH₂ and CH₃ in the branch chain), 1596 (phenyl group), 1478 (P–phenyl, CH₂ of spirocycle), 1410 (P–CH₂– of aliphatic), 1206 (P=O), 1014–1127 (Si–O–Si, P–O–C), 921 (P–O–phenyl). ¹H NMR (DMSO-*d*₆, ppm): −0.4 to 0.1 (Si–CH₃), 0.6 (C–CH₂–Si), 1.8–1.9 (−CH₂–P), 4.21–4.24 (−CCH₂O–PO–, 8H); ³¹P NMR (DMSO-*d*₆, ppm): 38–42 (P in phenyl group), −6.0 to −6.3 (P in the spirocycle). Figure 1b shows the synthesis route of the MWNT-g-SPDV samples. The MWNT–OH was firstly modified with APTES and MWNT–NH₂ was obtained; then the synthesized flame retardant SPDV was grafted onto the MWNT–NH₂ and the MWNT-g-SPDV was obtained. Figure 2 shows the infrared spectra of MWNT, MWNT-g-APS, and MWNT-g-SPDV. In the FTIR spectrum of MWNT-g-APS, the absorption peaks at 3515 cm^{-1} (−NH₂), 1024–1127 (Si–O–C) are found. In the FTIR spectrum of MWNT-g-SPDV, the absorption peaks at 3485 cm^{-1} (−NH), 3065 (C–H in phenyl group), 2780 (CH₂ and CH₃ in DV segment), 1650–1675 (−NH; phenyl group), 1460–1485 (P–phenyl, CH₂ in SPDPC segment), 1225 (P=O), 1045–1105 (Si–O–Si, P–O–C) are found. Comparing with the FTIR spectrum of MWNT-g-APS, we can find that the characteristic peaks of amino groups in APS died down and the new secondary amide appeared from the spectrum of MWNT-g-SPDV, demonstrating that the phosphorus acyl chloride groups on SPDV have reacted with amino groups of MWNT-g-APS. Figure 3 shows the ¹H NMR spectra of SPDV and MWNT-g-SPDV. The peaks of ¹H NMR (DMSO-*d*₆, ppm): −0.4 to

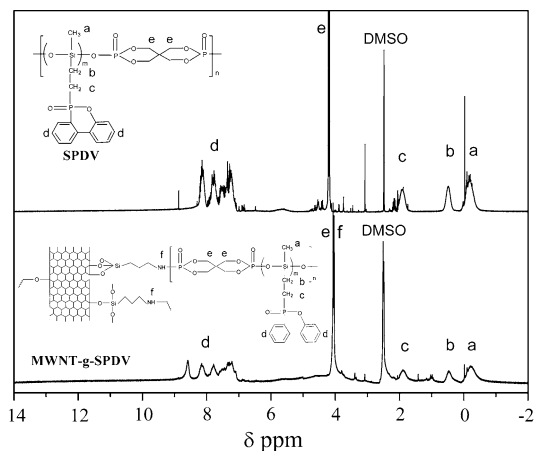


Fig. 3 ¹H NMR spectra of SPDV and MWNT-g-SPDV in DMSO-*d*₆

0.1 (Si–CH₃), 0.6 (C–CH₂–Si), 1.8–1.9 (−CH₂–P), 4.21–4.24 (−CCH₂O–PO–, 8H in the spiral structure), 7.2–8.6 (benzene ring) were found in ¹H NMR of both SPDV and MWNT-g-SPDV, while 4.02–4.08 (N–H) was found in ¹H NMR of MWNT-g-SPDV. The above results of FTIR and ¹H NMR clearly indicated that SPDV has been attached to the external walls of the functionalized MWNTs.

As an additional and more direct evidence for the covalent functionalization of SPDV onto MWNTs, the MWNTs and MWNT-g-SPDV were analyzed by TEM and the results are shown in Fig. 4. Figure 4a displays a typical TEM image of pristine MWNTs. The tubes possess uniform inner and outer diameters of about 5–10 and 10–20 nm in average along their length, respectively. The hollow core and the open ends can be seen in pristine MWNTs and the surface seems to be smooth and clear without any extra phase adhering to them. In contrast, the MWNT-g-SPDV sample can be easily distinguished from pristine MWNTs as the core–shell structure with the SPDV layer as the shell and MWNTs crystal sheet at the center are clearly discerned, and the thickness of the SPDV shell is about 5–8 nm in average shown in Fig. 4b. Undoubtedly, SPDV chains immobilized onto the surfaces of MWNTs.

The relative amounts of grafted SPDV in the MWNT-g-SPDV can be determined by TGA through the thermal decomposition of SPDV, because SPDV have a lower decomposition temperature than MWNTs. Figure 5 shows the thermograms of pristine MWNTs, MWNT-g-SPDV, and SPDV under N₂ atmosphere at a heating rate of 20 °C/min. Clearly, pristine MWNTs have good thermal stability under N₂ atmosphere. When the temperature is increased up to 800 °C, there is no obvious decomposition in pristine MWNTs and about 96 wt% residues are left. The synthesized P–Si containing flame retardant SPDV is an excellent carbonization agent and 36 wt% residue remains after thermal degradation at 800 °C. For MWNT-g-SPDV,

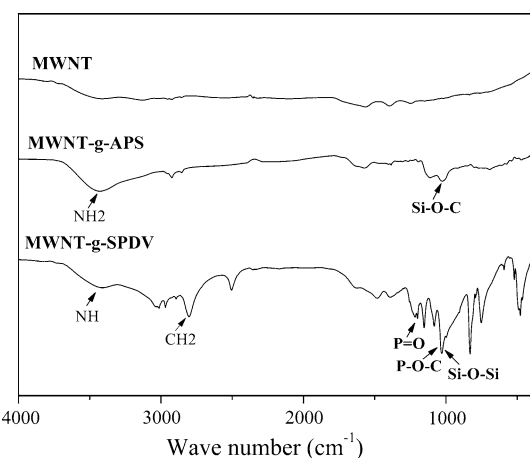


Fig. 2 FTIR spectra of MWNT, MWNT-g-APS, and MWNT-g-SPDV

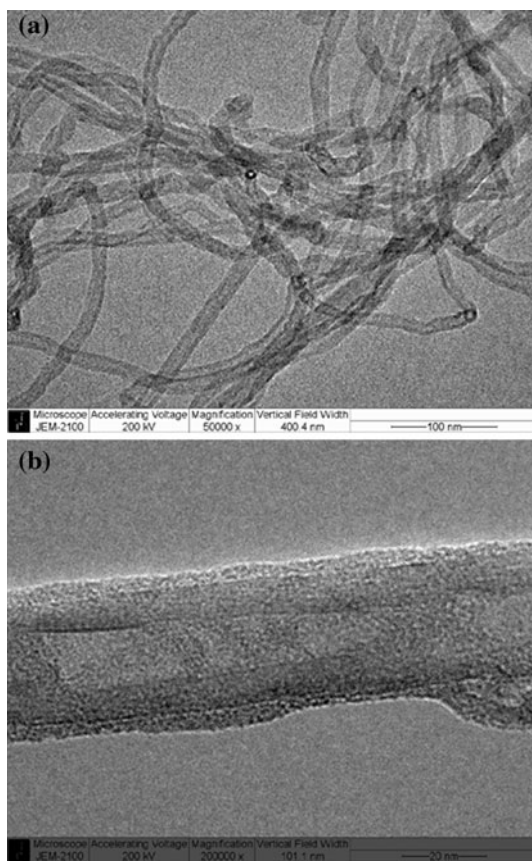


Fig. 4 TEM images of MWNT (a) and MWNT-g-SPDV (b)

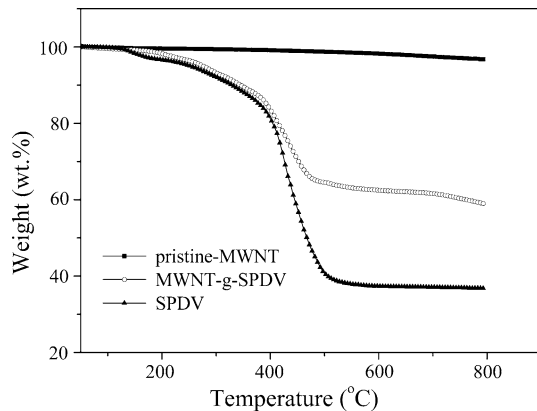


Fig. 5 TG curves versus temperature for MWNT, SPDV, and MWNT-g-SPDV under N_2 atmosphere

59 wt% char is left at the end of decomposition in this test. Therefore, the TGA results can be applied to estimate the relative amounts of the grafted SPDV onto the convex walls of MWNTs. The difference in the weight loss at 800 °C between pristine MWNTs, SPDV, and MWNT-g-SPDV can be calculated and shows that the SPDV grafting amount is about 61 wt%.

Morphology observation of EVM/MWNT nanocomposites

Figure 6a and b shows the TEM images of the EVM/MWNT (1.0 phr) and EVM/m-MWNT (1.0 phr) nanocomposites, respectively. MWNT-g-SPDV has been individually and disordered dispersed throughout the EVM matrix (Fig. 6b) compared with the pristine MWNTs (Fig. 6a), for which many large MWNTs aggregates are still visible. It can be concluded that the MWNT-g-SPDV obtains better dispersion in EVM matrix from microscopic scale. This drastic change in the quality of MWNT dispersion originates from the destruction of the native MWNT aggregates, which are thermodynamically stabilized by numerous $\pi-\pi$ electronic interactions between the CNTs; these $\pi-\pi$ electronic interactions are still present in the EVM matrix [32]. However, the modification of MWNTs with the flame retardant SPDV, allows the nanotubes' surface to be covered with a thin layer of SPDV, which impedes the formation of $\pi-\pi$ interactions

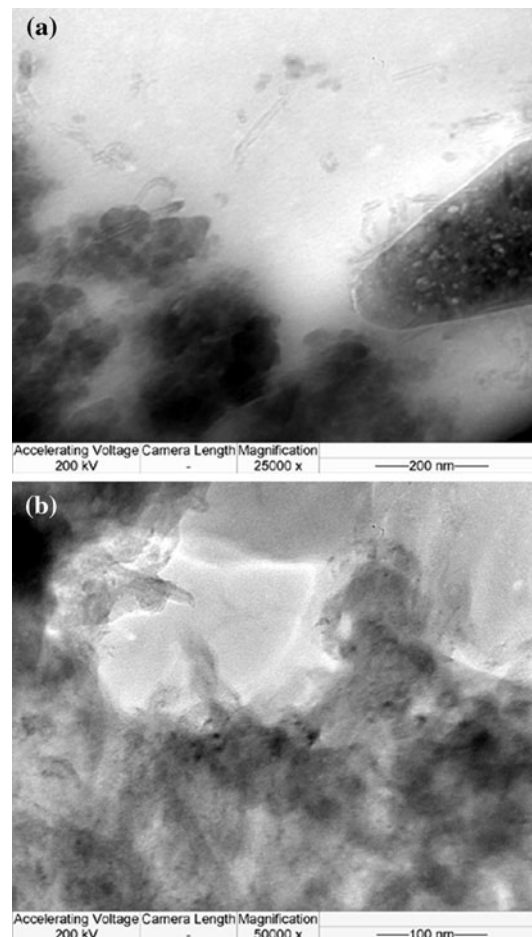


Fig. 6 TEM images of the EVM/MWNT (a) and EVM/MWNT-g-SPDV (b) nanocomposites

and improves the dispersion of MWNT-g-SPDV in EVM matrix shown in Fig. 6b.

Flammability of EVM/MWNT nanocomposites

The traditional method of measuring and predicting the fire hazard of materials is based on the determination of a variety of properties measured independently by different small-scale apparatuses, which can bring a larger difference with the actual situation in real fire. Cone calorimeter test based on the oxygen consumption principle, as a performance-based method, provides a means of measuring a number of different parameters in the same test and has been found to correlate well with those obtained from a large-scale fire test, which can be used to predict the combustion behavior of materials in a real fire [30, 33]. The cone calorimeter data for EVM and the two corresponding nanocomposites filled with either 1.0 phr MWNTs or 1.0 phr m-MWNTs are presented in Table 1 and Figs. 7, 8, 9, and 10. It can be found that the peak of heat release rate (PHRR) for the virgin EVM reaches a value of 836 kW/m², and which presents very sharp HRR curve and the combustion is complete after 300 s. The sample shows very strong bubbling and heavily melting during the combustion. Compared with neat EVM. The incorporation of 1.0 phr MWNTs (pristine and modified) leads to a strong reduction of PHRR, which reaches a value of 553 and 508 kW/m², respectively, and the reduction in PHRR was nearly 34 and 39%. The reduction of HRR was accompanied by a pronounced prolongation of burning time (from 327 to 545 s and 564 s, respectively). Moreover, it can be found (Table 1) that the average HRR (AHRR), total heat release (THR), and average effective heat of combustion (AEHC) decreases; the TTI increases (from 53 to 68 s and 71 s, respectively); the fire performance index (FPI) was significantly enhanced (from 0.063 m² s/kW to 0.123 and 0.139 m² s/kW, respectively) and the peak of smoke production rate (PSPR) was evidently reduced (from 0.156 to 0.105 m²/s and 0.113 m²/s, respectively) for the EVM/MWNTs and EVM/m-MWNTs nanocomposites compared with neat EVM matrix.

Table 1 Cone calorimeter results of unfilled EVM and the two related flame retardant nanocomposites at 35 kW/m²

Formulation	EVM	EVM + 1.0 phr MWNT	EVM + 1.0 phr m-MWNT
TTI (s)	53	68	71
PHRR (kW/m ²)	836	553	508
AHRR (kW/m ²)	416	292	274
THR (MJ/m ²)	101	93	91
FPI (m ² s/kW)	0.063	0.123	0.139
AEHC (MJ/kg)	33.2	28.6	28.3
PSPR (m ² /s)	0.156	0.105	0.113
Residues (%)	1.5	2.9	3.4

TTI time to ignition, *PHRR* peak of heat release rate, expressing the intensity of a fire, *FPI* fire performance index, the ratio of TTI and PHRR, *PSPR* peak of smoke production rate

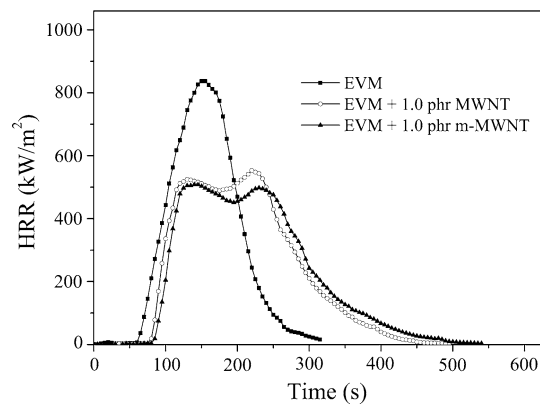


Fig. 7 HRRs versus burning time for neat EVM matrix and the according flame retardant nanocomposites

The dynamic curves of mass loss rate (MLR) present a very similar change with HRR curves shown as Fig. 8a. It can be found that the curves of residual mass become more flat for EVM/MWNTs and EVM/m-MWNTs nanocomposites shown as Fig. 8b and the final residual mass increases after combustion (from 1.5 to 2.9% and 3.4%, respectively) compared with neat EVM. An important charring effect is also observed from the photographs of residue after combustion for the EVM/MWNT and EVM/m-MWNT nanocomposites (Fig. 9b, c) compared with neat EVM (Fig. 9a). An interesting effect of the wrapping of the MWNTs by the thin layer of SPDV has been observed on the cohesion of the combustion residues shown in the photographs of Fig. 9. Compared to the EVM/MWNT material, the EVM/m-MWNT nanocomposites gives rise to a more cohesive and uniform carbonaceous residue. This better cohesion of the combustion residue of the nanocomposite based on m-MWNTs could be explained by the better dispersion of modified MWNTs. Figure 10a and b shows the SEM images of the residues after combustion for EVM/MWNTs and EVM/m-MWNTs nanocomposites with 1.0 phr loading, respectively. It can be seen that MWNTs show a similar network structure consisting of bundled conglomeration, and there are many pores within the network after combustion. However, the network formed by

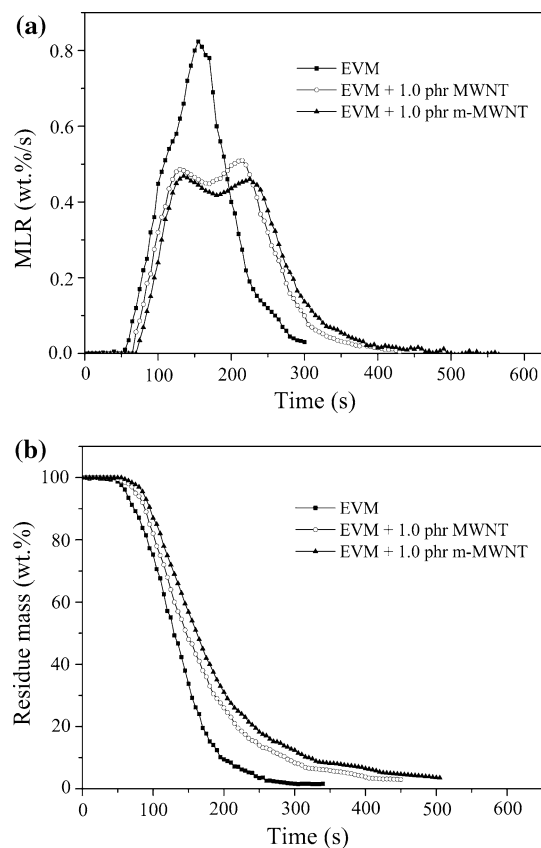


Fig. 8 MLRs (**a**) and residue mass (**b**) versus burning time for neat EVM matrix and the according flame retardant nanocomposites

the char of EVM/m-MWNTs nanocomposites is more compact and some other carbonaceous residues are left wrapping the MWNTs residue.

Compared to the virgin EVM, the EVM/MWNT and EVM/m-MWNT nanocomposites did not show any bubbling during the combustion probably because of the higher melt viscosity compared to the unfilled matrix. Such an increase in melt viscosity is clearly due to the presence of the MWNTs in the EVM matrix. Similar behavior has been reported for polymethylmethacrylate/SWNT nanocomposites by Kashiwagi et al. [25]. All the above changes indicate that the flame retardancy of EVM is improved obviously for the fillings of MWNTs or m-MWNTs. The better flame retardant improvement for the EVM/m-MWNT nanocomposites can be attributed to the better dispersion of MWNT-g-SPDV than pristine MWNT for the EVM/MWNT nanocomposites.

Mechanical properties of EVM/MWNT nanocomposites

The mechanical properties of EVM-based nanocomposites are closely related with the MWNTs dispersion condition.

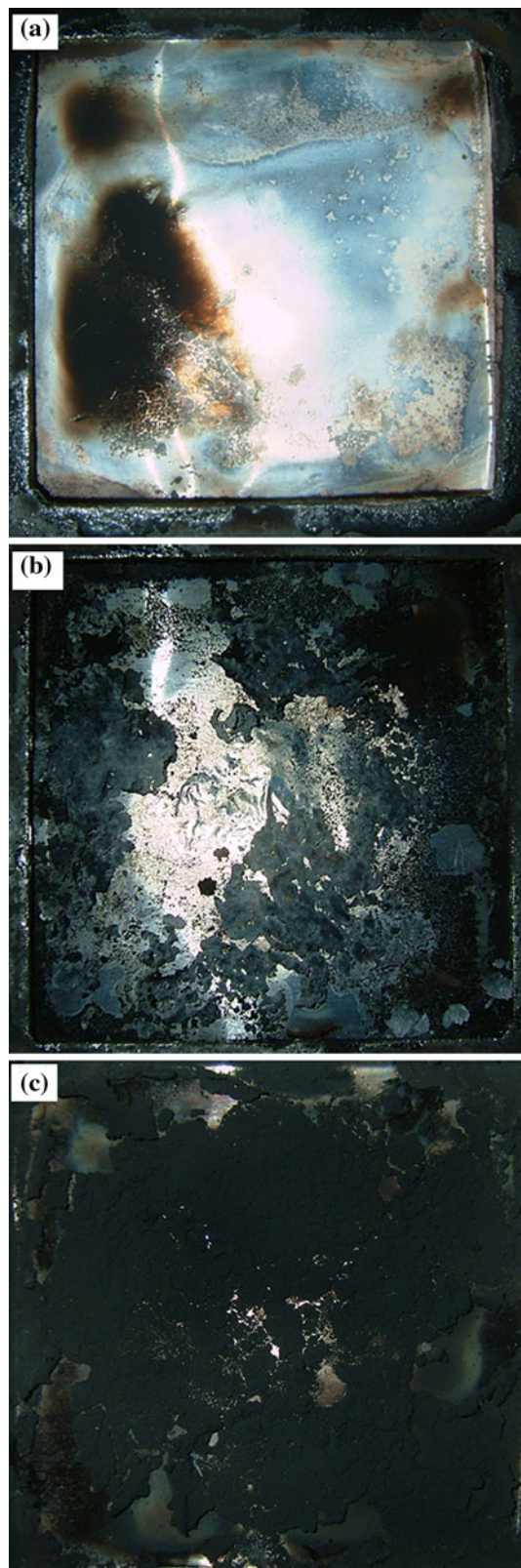


Fig. 9 Original residual photographs for the samples after combustion: **a** neat EVM; **b** EVM/MWNT 1.0 phr; **c** EVM/m-MWNT 1.0 phr

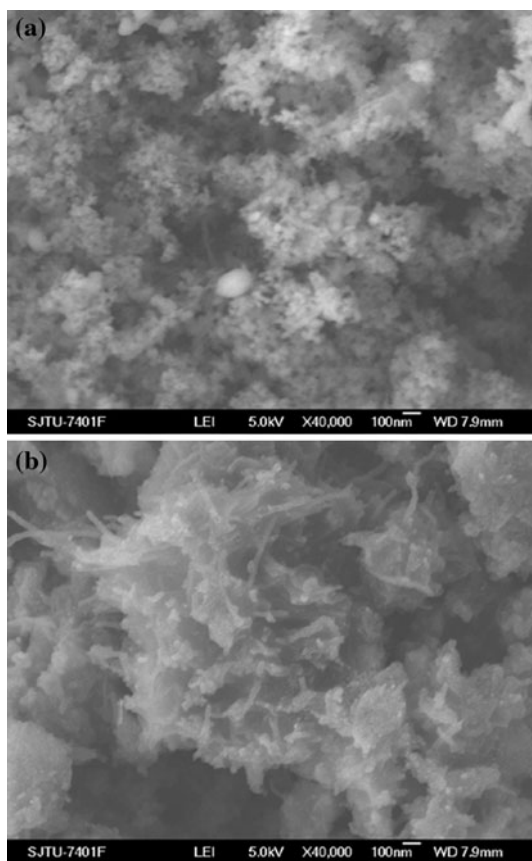


Fig. 10 The residual microstructure analysis after combustion for the samples of EVM/MWNT (a) and EVM/m-MWNT (b)

Table 2 Mechanical properties of neat EVM matrix and the according flame retardant nanocomposites

Formulation	Stress at break (MPa)	Elongation at break (%)	Young's modulus (MPa)
EVM	12.8 ± 1.1	552 ± 27	8.6 ± 0.9
EVM + 1.0 phr MWNTs	7.4 ± 1.3	347 ± 34	12.3 ± 1.2
EVM + 1.0 phr m-MWNTs	9.1 ± 1.2	365 ± 26	14.7 ± 1.1

Table 2 shows the mechanical test data for the different materials. The stress-strain curves of the EVM/MWNT and EVM/m-MWNT nanocomposites are similar in shape to those of the virgin EVM matrix, indicating that the addition of the MWNTs does not change the entire mechanical behavior of the EVM matrix. It can be found (Table 2) that the stress and elongation at break decrease and the Young's modulus increase (from 8.6 to 12.3 MPa and 14.7 MPa, respectively) after the incorporation of 1.0 phr MWNTs or 1.0 phr m-MWNTs to EVM matrix. Compared to the value of the neat EVM matrix, the stress at break and elongation at break of the EVM/MWNT nanocomposite decreases by 42 and 37%, respectively,

while the decrease recorded for the EVM/m-MWNT nanocomposite are limited to 29 and 34%, respectively. This is commonly what is observed for polymer-based nanocomposites filled with CNTs caused by different dispersion state in the matrix as reported by some researches [34–36].

Conclusions

A novel phosphorus–silicon containing flame retardant (SPDV) has been synthesized and covalently grafted onto the surfaces of MWNTs by the reaction of SPDV with MWNTs-NH₂. The evidence that SPDV are successfully grafted onto the surface of MWNTs is furnished by the results from FTIR, ¹H NMR, and TGA measurements. A core–shell nanostructure with MWNTs as the hard core and inhomogeneous flame retardant SPDV layers as the soft shell are observed by TEM images. Meanwhile, the TEM images show that the functionalized MWNTs with SPDV can achieve better dispersion in EVM matrix. Cone calorimeter test shows that the flame retardancy of EVM is evidently improved for the addition of MWNTs or m-MWNT: the PHRR, AHRR, THR, and AEHC decreases; the TTI, FPI and residual mass increases for the EVM/MWNTs and EVM/m-MWNTs nanocomposites compared to neat EVM. The reason may be that the movement of polymer chains is restricted by the presence of MWNTs and presents different behavior with nature of EVM matrix during combustion. The mechanical test shows that the stress and elongation at break decrease and the Young's modulus increase after the incorporation of MWNTs to EVM matrix. Anyway, the flammability and mechanical properties of the EVM/MWNTs nanocomposites are strongly dependent on the dispersion state of MWNTs.

References

- Iijima S (1991) Nature 56:354
- Kim JA, Seong DG, Kang TJ, Youn JR (2006) Carbon 44:1898
- Popov VN (2004) Mater Sci Eng 43:61
- Arun KK, Bani H, Cipriano MK, Duesterberg AL, Gershon DP, Srinivasa RR, Hugh AB (2007) Macromolecules 40:7400
- Du FM, Robert CS, Wei Z, Stijn B, John EF, Karen IW (2004) Macromolecules 37:9048
- Moniruzzaman M, Winey KI (2006) Macromolecules 39:5194
- Hirsch A (2002) Angew Chem Int Ed 41:1853
- Kim KH, Jo WH (2007) Macromolecules 40:3708
- Lee JU, Huh J, Kim KH, Park C, Jo WH (2007) Carbon 45:1051
- Xue CH, Zhou RJ, Shi MM, Gao Y, Wu G, Zhang ZB (2008) Nanotechnology 19:215604
- Xu GY, Wu WT, Wang YS, Pang WM, Zhu QR, Wang PH (2007) Nanotechnology 18:145606
- You YZ, Hong CY, Pan CY (2006) Nanotechnology 17:2350

13. Hong CY, You YZ, Pan CY (2006) *Polymer* 47:4300
14. Qin S, Qin D, Ford WT, Resasco DE, Herrera JE (2004) *J Am Chem Soc* 126:170
15. Kong H, Gao C, Yan D (2004) *J Am Chem Soc* 126:412
16. Jeon JH, Lim JH, Kim KM (2009) *Polymer* 50:4488
17. Baskaran D, Mays JW, Brather MS (2004) *Angew Chem Int Ed* 43:2138
18. Gao Y, Zhou YF, Yan DY (2009) *Polymer* 50:2572
19. Chen SM, Wu GZ, Liu YD, Long DW (2006) *Macromolecules* 39:330
20. Petrov P, Lou XD, Pagnoulle C, Jerome C, Calberg C, Jerome R (2004) *Macromol Rapid Commun* 25:987
21. Kashiwagi T, Du F, Douglas JF, Winey KI, Harris RH, Shields JR (2005) *Nat Mater* 4:928
22. Ma HY, Tong LF, Xu ZB, Fang ZP (2008) *Adv Funct Mater* 18:414
23. Beyer G (2005) *Fire Mater* 29:61
24. Costache MC, Wang DY, Heidecker MJ, Manias E, Wilkie CA (2006) *Polym Adv Technol* 17:272
25. Kashiwagi T, Du FM, Winey KI, Groth KM, Shield JR, Bellayer SP, Kim H, Douglas JF (2005) *Polymer* 46:471
26. Kashiwagi T, Grulke E, Hilding J, Groth K, Harris R, Butler K, Shields J, Kharchenko J, Douglas J (2004) *Polymer* 45:4227
27. Wang LC, Jiang JQ, Jiang PK, Yu JH (2010) *J Polym Res*, in press
28. Babrauskas V (1992) In: Babrauskas V, Grayson SJ (eds) *Heat release in fires*. Elsevier Applied Science Publishers, London, p 61
29. Reaction to fire tests—heat release, smoke production and mass loss rate—Part 1. Heat release rate (cone calorimeter method), ISO 5660-1: 2002; International Organization for Standardization, Geneva, Switzerland
30. Hirschler MM (1992) In: Babrauskas V, Grayson SJ (eds) *Heat release in fires*. Elsevier Applied Science Publishers, London, p 375
31. Mouritz AP, Mathys Z, Gibson AG (2006) *Heat release of polymer composites in fire*. *Compos Part A* 37:1040
32. Peeterbroeck S, Laoutid F, Taulemesse JM, Monteverde F, Lopez-Cuesta JM, Nagy JB, Alexandre M, Dubois P (2007) *Adv Funct Mater* 17:2787
33. Digges KH, Gann RG, Grayson SJ, Hirschler MM, Lyon RE, Purser DA, Quintiere JG, Stephenson RR, Tewarson A (2008) *Fire Mater* 32:249
34. Ciselli P, Zhang R, Wang ZJ, Reynolds CT, Baxendale M, Peijs T (2009) *Eur Polym J* 45:2741
35. Song YS, Youn JR (2005) *Carbon* 43:1378
36. Choi S, Jeong YJ, Lee GW, Cho DH (2009) *Fibers Polym* 10:513